

Effects of Airfoil Geometry and Mechanical  
Characteristics on the Onset of Flutter  
(As a Basis for Future Work on the Effects of  
Structural Polynomial Nonlinearities on the Flutter  
Boundary)

Udbhav Sharma  
gte271u@mail.gatech.edu

School of Aerospace Engineering  
Georgia Institute of Technology

December 10, 2004

## **Abstract**

This paper derives linear 2nd order ordinary differential equations describing the motion of a 2 dimensional airfoil allowing for 3 spatial Degrees of Freedom in airfoil angular rotation, vertical movement and control surface rotation. The equations of motion are derived from a conservative Euler-Lagrange formulation with the non-dissipative forcing functions arising from steady, incompressible, inviscid 2 dimensional aerodynamics incorporating results from Thin Airfoil Theory. The resulting model predicts undamped, increasing oscillations below a critical airflow speed called the flutter boundary. The paper shows how this speed can be predicted from the eigenvalues of the system. By changing certain airfoil geometrical and mechanical properties, it is demonstrated that it is possible to aeroelastically tailor the airfoil such that flutter is avoided for a given flight regime. The model adopted has been found deficient in its ability to predict a realistic flutter boundary. This problem is due to the absence of dissipative forces in the aerodynamics of the model. It has been suggested that the model can be made more realistic by incorporating unsteadiness into the aerodynamics of the system using results from Peters' finite state theory.

# 1 Introduction

Aeroelasticity studies the dynamics of an elastic body moving through a fluid and undergoing deformation due to aerodynamic forces. Aeroelastic considerations are of vital importance in the design of aerospacecraft because vibration in lifting surfaces, called *flutter*, can lead to structural fatigue and even catastrophic failure [1]. An important problem concerns the prediction and characterization of the so called flutter boundary (or speed) in aircraft wings. Classical aeroelastic theories [2] predict damped exponentially decreasing oscillations for an aircraft surface perturbed at speeds below the critical flutter boundary. However, exponentially increasing oscillations are predicted beyond this speed [3]. Therefore, knowledge of the stability boundary is vital to avoid hazardous flight regimes. This stability problem is studied in classical theories with the governing equations of motion reduced to a set of linear ordinary differential equations [2].

Linear aeroelastic models fail to capture the dynamics of the system in the vicinity of the flutter boundary. Stable limit cycle oscillations (LCO) have been observed in wind tunnel models [3] and real aircraft [1] at speeds in the neighborhood of the predicted flutter boundary. These so called "benign", finite amplitude, steady state oscillations are unfortunately not the only possible effect. Unstable LCO have also been noticed both *before* and *after* the onset of the predicted flutter speed [3]. In the case of unstable LCO, the oscillations grow suddenly to very large amplitudes causing catastrophic flutter and structural failure. A more accurate aeroelastic model will need to incorporate nonlinearities present in the system to account for such phenomena.

Nonlinear effects in aeroelasticity arise from either the aerodynamics of

the flow or from the elastic structure of the airfoil [3]. Sources of nonlinearity in aerodynamics include the presence of shocks in transonic and supersonic flow regimes and large angle of attack effects, where the flow becomes separated from the airfoil surface [3]. Structural nonlinearities are known to arise from freeplay or slop in the control surfaces, friction between moving parts and continuous nonlinearities in structural stiffness [3].

This paper is the first step in developing a structurally nonlinear aeroelastic model with unsteady aerodynamics. We first adopt a linear aerodynamic model that limits the ambient airflow to inviscid, incompressible (low Mach number) and steady state flow. A more sophisticated unsteady aerodynamic model such as Peters' finite-state Thin Airfoil Theory will be required to capture dissipative effects in flutter. Since we derive the structural equations separately from the aerodynamics, it will be simple to adopt more sophisticated aerodynamics at a later stage without affecting the structural model. Further development will include the addition of nonlinear polynomial terms to model structural stiffness coefficients once the unsteady model is in place.

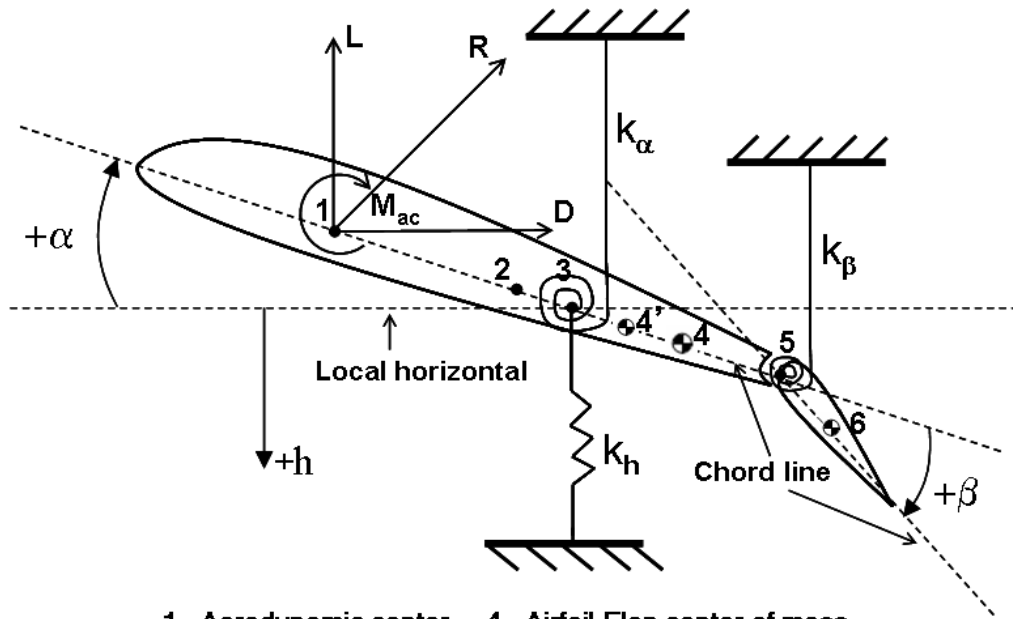
## 2 Equations of motion

The aeroelastic behavior of aircraft lifting surfaces has traditionally been studied with a simple 2 dimensional (2D) *typical airfoil section* model [2]. An airfoil section (or airfoil) is physically a cross section of a wing or other lifting surface. The flow around this section is assumed to be representative of the flow around the wing. Since the airfoil section is modeled as a rigid body, elastic deformations due to structural bending and torsion are modeled by springs attached to the airfoil [1]. The use of an airfoil model

is consistent with standard aerodynamic analysis where the flow over 3D lifting surfaces is first studied using a cross section and the results are then suitably modified to account for 3D (finite wing) effects [4]. In this study, finite wing corrections are not incorporated into the aerodynamic model.

A brief discussion of airfoil terminology will be useful at this point. The tip of the airfoil facing the airflow is called the leading edge (LE) and the end of the airfoil is called the trailing edge (TE). The straight line distance from the LE to the TE is called the *chord* of the airfoil. The airfoil chord is fixed by the type of airfoil specified, given by standard NACA nomenclature [5] and hence can be used as a universal reference length. The *mean camber line* is the locus of points midway between the upper and lower surfaces of the airfoil. For a symmetrical airfoil, the mean camber line is coincident with the chord line.

The typical airfoil section studied in this paper includes a TE control surface known as a flap (see Fig. 1). As an airfoil moves through a flow, it has potentially an infinite number of spatial Degrees of Freedom (DOF). Here, the airfoil is constrained to one translational and two rotational DOF (Fig. 1). The translational DOF called *plunging* is the vertical movement of the airfoil about the local horizontal with a displacement  $h = h(t)$  ( $t$  denotes dimensional time). The rotational or *pitching* DOF of the airfoil about the elastic center (point 3 in Fig. 1) is represented by the angle  $\alpha = \alpha(t)$  measured counterclockwise from the local horizontal. Finally, the rotational or *flapping* DOF of the flap about its hinge axis (point 5 in Fig. 1) is measured by the angle  $\beta = \beta(t)$ , with the airfoil chord line as a reference. The elastic constraints on the airfoil are represented by one translational and two rotational springs with stiffness coefficients  $k_h$ ,  $k_\alpha$  and  $k_\beta$  (treated for now as constants, but developed further in future work).



- |                               |  |
|-------------------------------|--|
| <b>1 - Aerodynamic center</b> | <b>4 - Airfoil-Flap center of mass</b> |
| <b>2 - Half chord point</b>   | <b>5 - Flap pivot point</b>            |
| <b>3 - Axis of rotation</b>   | <b>6 - Flap center of mass</b>         |

Figure 1: Typical Airfoil Section. See Table 1 for nomenclature. Also see Fig. 2 for definition of geometrical constants.

Points of interest on the airfoil section that appear throughout the paper are shown in Fig. 2. The center of pressure for the airfoil lies at Point 1, also called the aerodynamic center (also see section 3). Point 2 is the half chord point of the airfoil section. One half of the chord length ( $b$  in Fig. 2) is used in this paper to non-dimensionalize the other geometrical lengths of the airfoil. The half chord also comes up while formulating the aerodynamic forces and moments (see section 3). Two important reference points are the elastic center, point 3, about which the airfoil rotates and the flap hinge location, point 5, about which the TE flap rotates. The center of gravity (CG) locations are at points 4 (airfoil and flap), 4' (airfoil alone) and 6

(flap alone). The geometrical constants relating these points are defined graphically in Fig. 2 and summarized in Table 1.

The classical aeroelastic equations of motion for a typical airfoil section were derived by Theodorsen [2] using a force balance. The equations are derived in this paper by writing non-conservative Euler-Lagrange equations of motion for each DOF. The aerodynamic force and moments (see section 3) associated with the airfoil are treated as external forces in the Euler - Lagrange formulation. Three right handed cartesian coordinate frames are used in the following derivation - an inertial frame  $I(\hat{i}_1, \hat{i}_2, \hat{i}_3)$  with its origin at the half chord and two airfoil fixed frames. The first airfoil-fixed frame  $A(\hat{a}_1, \hat{a}_2, \hat{a}_3)$  also has its origin at the airfoil half chord. The points of interest 1–5 in Fig. 2 on the chord line are coincident with the  $\hat{a}_1$  direction. The second non-inertial frame  $B(\hat{b}_1, \hat{b}_2, \hat{b}_3)$  has its origin at the flap pivot point with the flap center of mass lying in the  $\hat{b}_1$  direction. The  $\hat{a}_1$  and  $\hat{b}_1$  axes are coincident with the inertial  $\hat{i}_1$  axis for the airfoil in its non-deflected position. The general rotations to transform a vector  $\vec{v}$  from frames  $A, B$  into the inertial reference frame  $I$  are given by [6]

$$\{\vec{v}\}_I = [\mathbf{R}_z(-\alpha)]\{\vec{v}\}_A \quad \text{where} \quad \{\vec{v}\}_I = [\mathbf{R}_z(-\alpha - \beta)]\{\vec{v}\}_B \quad (1)$$

where  $[\mathbf{R}_z(\psi)]$  denotes the first Euler rotation matrix for an angle  $\psi$ . We note that the rotations are considered small and hence small angle approximations are used i.e. *sine* and *cosine* functions are approximated to the first term in their respective Taylor series.

The Lagrangian is the difference between the kinetic  $\mathcal{T}$  and potential  $\mathcal{V}$  energies of the system,  $\mathcal{L} = \mathcal{T} - \mathcal{V}$ . By defining the gravitational potential datum line at the  $\hat{i}_1$  inertial axis (see Fig. 2) and arguing that the movement of the CG of the airfoil about this line is small, the contribution of

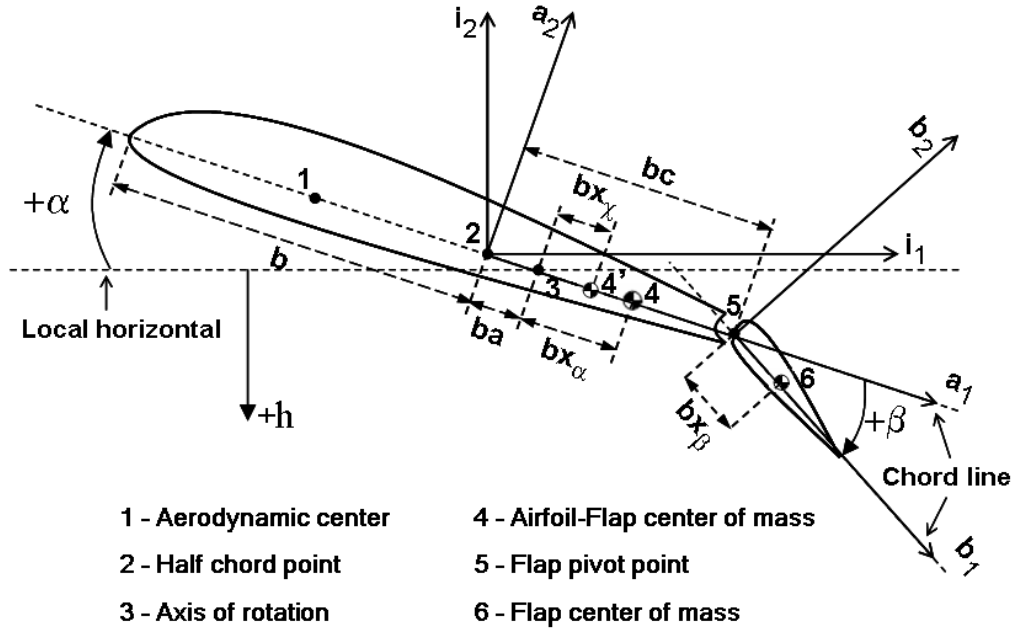


Figure 2: Typical airfoil section showing inertial and airfoil-fixed axes and geometrical constants. See Table 1 for definition of terms. Also see Fig. 1 for definition of aerodynamic forces and elastic constraints.

gravitational potential to the energy of the system can be neglected. Then, the potential energy of the system is,

$$\mathcal{V} = \frac{1}{2}k_\alpha \alpha^2 + \frac{1}{2}k_\beta \beta^2 + \frac{1}{2}k_h h^2 \quad (2)$$

The expression for the kinetic energy in terms of the velocities  $v_j$ ,  $j = \{4', 6\}$  of the mass centers (points 4' and 6 in Fig. 2) and the angular rotations  $\alpha$  and  $\beta$  is,

$$\mathcal{T} = \frac{1}{2}I_a \dot{\alpha}^2 + \frac{1}{2}I_f (\dot{\alpha} + \dot{\beta})^2 + \frac{1}{2}m_a \vec{v}_{4'} \cdot \vec{v}_{4'} + \frac{1}{2}m_f \vec{v}_6 \cdot \vec{v}_6 \quad (3)$$

Here,  $m_j$ ,  $j = \{a(\text{airfoil}), f(\text{flap})\}$  are the masses and  $I_j$ ,  $j = \{a(\text{airfoil}), f(\text{flap})\}$  are the moments of inertia referred to the CG locations.

The velocities of the mass centers can be written relative to the rotation centers (points 3 and 5 in Fig. 2) as,

$$\begin{aligned}\vec{v}_{4'} &= \vec{v}_3 + (-\dot{\alpha})\hat{a}_3 \times \vec{r}_{34'} \\ \vec{v}_6 &= \vec{v}_5 + (-\dot{\beta})\hat{b}_3 \times \vec{r}_{56} + (-\dot{\alpha})\hat{a}_3 \times \vec{r}_{35}\end{aligned}\quad (4)$$

The length of the vectors  $r_{ij}^{\vec{}}$  can be obtained from Fig. 2. Performing rotations into the inertial reference frame using equation (1) with small angle approximations and taking the cross products in the above equation,

$$\begin{aligned}\vec{v}_{4'} &= -[bx_\chi \alpha \dot{\alpha}] \hat{i}_1 - [\dot{h} + bx_\chi \dot{\alpha}] \hat{i}_2 \\ \vec{v}_6 &= -[bx_\beta(\alpha + \beta) \dot{\beta} + b(c-a)\alpha \dot{\alpha}] \hat{i}_1 - [\dot{h} + bx_\beta \dot{\beta} + b(c-a)\dot{\alpha}] \hat{i}_2\end{aligned}$$

Finally, noting again that  $\alpha$  and  $\beta$  are small, we keep only the terms that are linear in  $\alpha$  and  $\beta$  in the above equation,

$$\begin{aligned}\vec{v}_{4'} \cdot \vec{v}_{4'} = |\vec{v}_{4'}|^2 &= (\dot{h} + bx_\chi \dot{\alpha})^2 \\ \vec{v}_6 \cdot \vec{v}_6 = |\vec{v}_6|^2 &= (\dot{h} + bx_\beta \dot{\beta} + b(c-a)\dot{\alpha})^2\end{aligned}\quad (5)$$

Substituting equations (5) into the kinetic energy expression from (3) we have,

$$\begin{aligned}\mathcal{T} &= \frac{1}{2} [I_a + I_f + m_a b^2 x_\chi^2 + m_f b^2 (x_\beta + c - a)^2] \dot{\alpha}^2 + \frac{1}{2} [I_f + m_f b^2 x_\beta^2] \dot{\beta}^2 + \\ &+ \frac{1}{2} [m_a + m_f] \dot{h}^2 + [I_f + m_f b^2 x_\beta^2 + (m_f b^2 x_\beta)(c - a)] \dot{\alpha} \dot{\beta} + \\ &+ [m_a b x_\chi + m_f b (x_\beta + c - a)] \dot{h} \dot{\alpha} + m_f b x_\beta \dot{\beta} \dot{h}\end{aligned}\quad (6)$$

We note here that from Fig. 2 the CG location of the airfoil-flap combination can be expressed in terms of the CG locations of the airfoil and flap as  $(m_a + m_f)bx_\alpha = m_a bx_\chi + m_f b(x_\beta + c - a)$ . Then, the following structural

Table 1: Nomenclature

<b>Variables</b> (see Fig. 1)	
$\alpha$	Pitch angle (Positive counterclockwise)
$h$	Plunging displacement (Positive downwards)
$\beta$	Flap angle (Positive counterclockwise)
<b>Aerodynamic Forces/Moments</b> (see Fig. 2)	
$L$	Resultant aerodynamic force at point 1
$M_\alpha$	Moment due to L about point 3
$M_\beta$	Moment due to L about point 5
<b>Structural Constants</b>	
$b$	Half-chord of airfoil
$m$	Airfoil mass per unit length
$I_i$	Moments of inertia, $i = \{\alpha (air\ foil), \beta (flap)\}$
$S_i$	Static moments, $i = \{\alpha (air\ foil), \beta (flap)\}$
$k_i$	Elastic constraint stiffness, $i = \{\alpha, \beta, h\}$ (see Fig. 2)
<b>Geometrical Constants</b> (Non-dimensional)	
$a$	Coordinate of axis of rotation (elastic center)
$c$	Coordinate of flap hinge
$x_\alpha$	Distance of airfoil-flap mass center from a
$x_\chi$	Distance of airfoil mass center from a
$x_\beta$	Distance of flap mass center from c

quantities that appear in Theodorsen's form of the equations [2] are defined.

$$\begin{aligned}
m &= m_a + m_f \\
I_\alpha &= I_a + I_f + m_a b^2 x_\chi^2 + m_f b^2 (x_\beta + c - a)^2 \\
I_\beta &= I_f + m_f b^2 x_\beta^2 \\
S_\alpha &= m_a b x_\chi + m_f b (x_\beta + c - a) = (m_a + m_f) b x_\alpha = m b x_\alpha \\
S_\beta &= m_f b x_\beta
\end{aligned} \tag{7}$$

The moments of inertia  $I_j$ ,  $j = \{\alpha(\text{airfoil}), \beta(\text{flap})\}$  and the static moments  $S_j$ ,  $j = \{\alpha(\text{airfoil}), \beta(\text{flap})\}$  in the above expressions are referred to the reference points (points 3(airfoil) and 5(flap) in Fig. 2). Then, the Lagrangian function in terms of the potential and kinetic energy expressions from (2) and (6), with the structural quantities as defined in (7) is,

$$\begin{aligned} \mathcal{L} = & \left\{ \frac{1}{2} I_\alpha \dot{\alpha}^2 + \frac{1}{2} I_\beta \dot{\beta}^2 + \frac{1}{2} m \dot{h}^2 + [I_\beta + b(c-a)S_\beta] \dot{\alpha}\dot{\beta} + S_\alpha \dot{h}\dot{\alpha} + S_\beta \dot{\beta}\dot{h} \right\} \\ & - \frac{1}{2} \{k_\alpha \alpha^2 + k_\beta \beta^2 + k_h h^2\} \end{aligned} \quad (8)$$

The general expression for the non-conservative form of the Euler-Lagrange equations is [6],

$$\frac{d}{dt} \left( \frac{\partial L}{\partial \dot{q}_i} \right) - \frac{\partial L}{\partial q_i} = Q_i, \quad i = 1, \dots, n \quad (9)$$

We choose  $n = 3$  and  $i = \alpha, \beta, h$  for the coordinates. Let  $Q_i$ ,  $i = \{\alpha, \beta, h\}$  represent the generalized forces on the RHS of the equation. The external forces on the airfoil arise due to the force  $\vec{R}$  and the moment  $\vec{M}_{ac}$  (see Fig. 1). The force  $R$  produces moments about our reference points 3, 5 which we shall call  $\vec{M}_\alpha$ ,  $\vec{M}_\beta$  using the notation of Theodorsen [2]. The generalized forces can then be obtained from a variational principle called the principle of virtual work (PVW) [6], which states that the external forces  $\vec{Q}_i$  on a system produce no virtual work  $\delta W$  for virtual displacements  $\delta \vec{q}_i$ . The mathematical statement for the principle is,

$$\delta W = \sum_{i=1}^n \vec{Q}_i \cdot \delta \vec{q}_i = 0 \quad (10)$$

The virtual displacements of a point on the airfoil can be written as  $-\delta h \hat{\mathbf{i}}_2$ ,  $-\delta \alpha \hat{\mathbf{i}}_3$  and  $-\delta \beta \hat{\mathbf{i}}_3$  in the inertial frame  $I$ . Then the general statement of

PVW from equation (10) gives,

$$\begin{aligned}
\delta W &= \vec{R} \cdot (-\delta h \hat{\mathbf{i}}_2) + \vec{M}_\alpha \cdot (-\delta \alpha \hat{\mathbf{i}}_3) + \vec{M}_\beta \cdot (-\delta \beta \hat{\mathbf{i}}_3) = 0 \\
\Rightarrow \delta W &= L \hat{\mathbf{i}}_2 \cdot (-\delta h \hat{\mathbf{i}}_2) + (-M_\alpha \hat{\mathbf{i}}_3) \cdot (-\delta \alpha \hat{\mathbf{i}}_3) + (-M_\beta \hat{\mathbf{i}}_3) \cdot (-\delta \beta \hat{\mathbf{i}}_3) = 0 \\
\Rightarrow \delta W &= -L \delta h + M_\alpha \delta \alpha + M_\beta \delta \beta = 0
\end{aligned} \tag{11}$$

which gives us the expressions for the generalized forces in terms of aerodynamic lift and moments,

$$Q_\alpha = M_\alpha, Q_\beta = M_\beta \text{ and } Q_h = -L$$

The Lagrangian (8) is substituted in equations (9) along with the relationships for the generalized forces given above. Evaluating the expressions gives three 2nd order ordinary differential equations (ODE) as they appeared originally in Theodorsen's paper [2],

$$\begin{aligned}
I_\alpha \ddot{\alpha} + (I_\beta + b(c-a)S_\beta) \ddot{\beta} + S_\alpha \ddot{h} + k_\alpha \alpha &= M_\alpha \\
I_\beta \ddot{\beta} + (I_\beta + b(c-a)S_\beta) \ddot{\alpha} + S_\beta \ddot{h} + k_\beta \beta &= M_\beta \\
m \ddot{h} + S_\alpha \ddot{\alpha} + S_\beta \ddot{\beta} + k_h h &= L
\end{aligned} \tag{12}$$

The left hand side (LHS) of equations (12) represent the contributions from the structural dynamics of the airfoil. The right hand side terms (RHS) represent the aerodynamic forcing terms, which arise from the interaction of the airfoil with the moving flow around it. In the Theodorsen paper [2] the aerodynamic forcing terms on the RHS were expressed as linear functions of  $(\alpha, \dot{\alpha}, \ddot{\alpha}, \beta, \dot{\beta}, \ddot{\beta}, h, \dot{h}, \ddot{h})$ . These functions arose from the aerodynamic model chosen by Theodorsen, which assumed a thin airfoil limited to small oscillations in an unsteady incompressible flow. The equations (12) do not include any nonlinearities and assume constant stiffness coefficients  $k_i$ .

We develop a simple steady state aerodynamic model in the next section with a restriction of incompressibility and irrotationality for a thin airfoil undergoing small amplitude oscillations. This will lead to the basic steady linear model for our system. Future work will incorporate more sophisticated unsteady aerodynamics. Nonlinearities will be introduced in the unsteady model by replacing the stiffness coefficients with polynomial stiffness terms in future work.

### 3 Steady Aerodynamic Model

The terms on the right hand side of equations (12) represent the restoring aerodynamic force and moments on the airfoil. An aerodynamic model is needed to derive expressions for these in terms of the system variables  $\alpha$ ,  $\beta$  and  $h$ . As an airfoil moves through the air, there exists a pressure distribution around it, which can be integrated over its surface to give a single resultant force  $R$  and a moment  $M_{ac}$  acting at the aerodynamic center (point 1 in Fig. 1).

Consider an airfoil control mass (CM) enclosed in a control volume (CV)  $V$ , with control surface  $S$  in an inertial reference frame  $(x, y, z)$  (see Fig. 3). The airfoil CM is attached to an airfoil-fixed right handed cartesian reference frame  $(\tilde{x}, \tilde{y}, \tilde{z})$  moving in time  $t$ . The airfoil CM has constant mass  $m$  and velocity  $\vec{v} = \vec{v}(t)$ . The flow field enclosed in the CV around the airfoil is variable with both space and time. Its density is  $\rho = \rho(\vec{x}, t)$  and velocity is  $\vec{v} = v_x(\vec{x}, t)\hat{i} + v_y(\vec{x}, t)\hat{j} + v_z(\vec{x}, t)\hat{k}$ , defined in the inertial reference frame. The airfoil has a pressure distribution due to the flow field given by  $p = p(\vec{x}, t)$ . We wish to relate the time variable properties of the airfoil CM viewed from a Lagrangian frame (moving with the airfoil) to the proper-



For momentum conservation laws the continuum property of interest is momentum. We let  $\Psi = m\vec{v}$  and correspondingly  $\psi = \vec{v}$ . Then, substituting this in the RTT equation (13),

$$\frac{d}{dt} \iiint_{CM} m\vec{v} dV = \frac{d}{dt} \iiint_V \rho\vec{v} dV + \iint_S \rho\vec{v} (\vec{v} \cdot d\vec{S}) \quad (15)$$

The LHS of equation (15) Newton's 2nd Law (constant mass) relates the momentum of the airfoil CM to the force it experiences,

$$\vec{F} = m \frac{d}{dt}(\vec{v}) \quad (16)$$

The force  $\vec{F}$  on the airfoil CM is split into a volume force  $\vec{f}$  acting on a unit elemental volume  $dV$ , a force due to viscous shear stresses, represented simply by  $\vec{F}_{viscous}$  and a pressure force  $p$  acting on an elemental area  $dS$ . Then, for the control volume  $V$  and control surface  $S$ , equation (15) gives,

$$- \iint_S p d\vec{S} + \iiint_V \rho\vec{f} dV + \vec{F}_{viscous} = \frac{\partial}{\partial t} \iiint_V \rho\vec{v} dV + \iint_S (\rho\vec{v} \cdot d\vec{S}) \vec{v} \quad (17)$$

The continuity and momentum conservation equations do not have closed form solutions. To find closed form solutions to the equations, we impose certain conditions on the flow properties. First, the flow around the airfoil is assumed to be changing so slowly that a steady state in time can be assumed. Second, the flow is assumed to be incompressible (a good approximation [4] for a flow Mach number  $M < 0.3$ ) making  $\rho = \rho_\infty$  a constant, where the subscript  $\infty$  refers to freestream flow, far from the airfoil. Then, with these assumptions and applying the divergence theorem to the continuity equation (14),

$$\begin{aligned} \rho_\infty \iint_S (\vec{v} \cdot d\vec{S}) &= \rho_\infty \iiint_V (\vec{\nabla} \cdot \vec{v}) dV = 0 \\ \Rightarrow \vec{\nabla} \cdot \vec{v} &= 0 \end{aligned} \quad (18)$$

The third assumption is of irrotational flow which implies that the curl of the velocity field  $\vec{\nabla} \times \vec{v} = 0$ . This allows us to define a *potential* flow such that the velocity of the flow at every point is the gradient of a scalar potential function  $\phi(x, y, z)$ :

$$\vec{\nabla} \times \vec{v} = 0 \Leftrightarrow \vec{v} = \vec{\nabla}\phi(x, y, z). \quad (19)$$

Immediately, from equations (18, 19) we obtain Laplace's equation [4], governing incompressible, irrotational flow.

$$\nabla^2\phi = 0 \quad (20)$$

Since the equation is linear, a complicated flow about an airfoil can be broken into several elementary potential flows that are solutions to Laplace's equation. This is the basis for Thin Airfoil Theory [8, 9] which we shall use later. There are two boundary conditions [4] associated with equation (20) for the case of flow over a solid body. The first assumes that perturbations go to zero far from the body. Thus, we can define the freestream flow conditions as being *uniform* [4] i.e.  $\vec{v} = v_\infty \hat{i}$ . The second is the flow tangency condition for a solid body, which states that its physically impossible for a flow to cross the solid body boundary i.e.  $\vec{\nabla}\phi \cdot \hat{n} = 0$ .

Now we take a look at the momentum conservation equation (17). The irrotationality and incompressibility criteria imply that the flow is inviscid i.e. friction, thermal conduction and diffusion effects are not present (these effects are negligible for high Reynolds numbers associated with aircraft flight [4]). We have already neglected inertial forces in our derivation of the Euler-Lagrange equations and thus,  $\vec{f} = 0$ . For the 2-dimensional airfoil case, with unit depth in the z direction and the integration contour C defined

as shown in Fig. 3, equation (17) then reduces to:

$$-\oint_C p d\vec{S} = \rho_\infty v_\infty \oint_C (\vec{v} \cdot d\vec{S}) \quad (21)$$

The LHS represents the force  $R$  due to the pressure distribution on the airfoil. An expression for this can be calculated from either of the two integrals in equation (21). However, since we have assumed incompressible, irrotational flow, we can take advantage of the Kutta-Juokowski Theorem [4] that relates the force ( $R$ ) experienced by a two dimensional body of arbitrary cross sectional area immersed in an incompressible, irrotational flow to the magnitude of the circulation  $\Gamma$  around the body. Mathematically the Kutta-Juokowski Theorem states,

$$\vec{R} = \rho_\infty v_\infty^2 \times \vec{\Gamma}, \quad \text{where} \quad \vec{\Gamma} = -\oint_C (\vec{v} \cdot d\vec{S}) \quad (22)$$

Before moving onto Thin Airfoil Theory [8, 9], a brief discussion of the inviscid flow assumption is in order. The condition of non-viscous flow follows directly from the condition of irrotationality as a consequence of Kelvin's Theorem [4]. Kelvin's theorem proves that for an inviscid flow, with conservative body forces (in our case, body forces are zero), the circulation remains constant along a closed contour. This implies that there is no change in the vorticity,  $\vec{\nabla} \times \vec{v}$ , with time:

$$\frac{d\Gamma}{dt} = -\frac{d}{dt} \oint_C (\vec{v} \cdot d\vec{S}) = -\frac{d}{dt} \iint_S (\vec{\nabla} \times \vec{v}) \cdot d\vec{S} = 0 \quad (23)$$

If the vorticity is zero to begin with (as is the case for irrotational flow), in the absence of inviscid forces the flow will remain irrotational. The major drawback of ignoring viscosity is that zero drag is predicted for the airfoil (d'Alembert's paradox [4]). The paradox is apparent from equation (22). The lift force  $L$  is defined as always being normal to the free stream while

the drag force  $D$  is always parallel to the flow (See Fig. 1). Taking force components normal and parallel to the freestream flow,

$$\begin{aligned} L &= \rho_\infty |v_\infty^{\vec{}}| |\vec{\Gamma}| \sin\left(\frac{\pi}{2}\right) = \rho_\infty v_\infty \Gamma \\ D &= \rho_\infty |v_\infty^{\vec{}}| |\vec{\Gamma}| \sin(0) = 0 \end{aligned} \tag{24}$$

This paradox is resolved with the justification that the drag force is always parallel to the translational DOF for the airfoil  $h$  and can thus be safely ignored in our equations of motion. The line of action of the drag force rotates about the mean chord line, but since we are assuming small oscillations, any moments that could affect the two rotational DOF  $\alpha$  and  $\beta$  are neglected.

Classical Thin Airfoil Theory [8, 9] assumes that the flow around an airfoil can be described by the superposition of two potential flows, such that the entire flow around the airfoil has a velocity potential function that is a solution to Laplace's equation (20). The first potential flow is a uniform freestream flow that we have already described,  $\vec{v} = v_\infty \hat{i}$ . To this is added a second component of velocity, induced by the presence of the airfoil in the moving flow.

The fundamental assumption of the theory is that the velocity induced by the airfoil is equivalent to the sum of induced velocities of a line of elemental vortices, called a vortex sheet, placed on the chord line of the airfoil (see Fig. 4). Thus, the airfoil itself can be replaced by the vortex sheet in the model. In reality, there is a thin layer of high vorticity on the surface of the airfoil due to viscous effects and thus this model is somewhat justified, with the restriction that the airfoil be thin enough to model with just the chord line. The NACA [5] standard definition for a thin airfoil is that the thickness be no greater than 10% of the chord i.e.  $t_{max} \leq 0.1(2b)$ , where

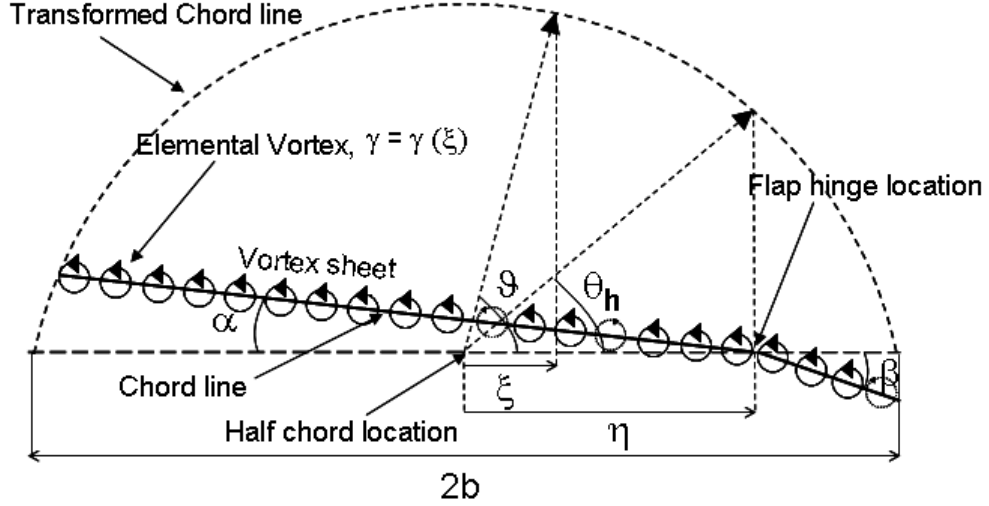


Figure 4: The airfoil is replaced with a vortex sheet along its chord line. The chord line is transformed to a half circle by the conformal map  $\xi = b(1 - \cos(\vartheta))$ . The flap location  $\eta$  is mapped to an angle  $\theta_h$ .

We state here explicitly that the vortex sheet is not a consequence of viscous effects, which we have ignored, but is a mathematical device to model the induced flow over a real airfoil. Replacing the airfoil with an equivalent vortex sheet on the mean chord line (Fig. 4) produces a velocity distribution consistent with vortex flow, which is a potential flow and hence satisfies Laplace's equation (20). The strength of each elemental vortex located at a distance  $dx$  is  $\gamma = \gamma(x)$ . The circulation around the airfoil is given by the sum of all the elemental vortices:

$$\Gamma = \int_0^{2b} \gamma(\xi) d\xi \quad (25)$$

The mean chord line of the airfoil is transformed via a conformal map [8] such that the airfoil coordinate  $\xi$  (see Fig. 4) is replaced by an angle  $\vartheta$ . The flap hinge coordinate  $\eta$  is transformed to the angle  $\theta_h$  (see Fig. 4). The

conformal map is given by the equation:

$$\xi = b(1 - \cos(\vartheta)) \quad (26)$$

where, the flap hinge location in Fig. 4 is given by  $\eta = b(1 - \cos(\theta_h))$ .

The lift per unit span,  $L = \rho_\infty v_\infty \Gamma$  follows from the Kutta-Joukowski Theorem (22). At this point, it is convenient to introduce a dimensionless variable known as the section lift coefficient [4], defined as,

$$c_l = \frac{L}{\frac{1}{2}\rho_\infty v_\infty^2 (2b)} = \frac{L}{b\rho_\infty v_\infty^2} = \frac{\Gamma}{bv_\infty} \quad (27)$$

where  $b$  is the half chord length from Fig. 2. From the Buckingham Pi theorem [4], in general for a given flow  $c_l = c_l(\alpha, \beta)$ . Expanding this with a first order Taylor approximation,

$$c_l = c_l(0, 0) + \frac{\partial c_l}{\partial \alpha} \alpha + \frac{\partial c_l}{\partial \beta} \beta \quad (28)$$

Thin airfoil theory [8] gives constant expressions for the partial derivatives in equation (28). We are assuming a symmetric airfoil, which makes  $c_l(0, 0) = 0$  [4]. Then,

$$c_l = [2\pi] \alpha + 2[(\pi - \theta_h) + \sin(\theta_h)] \beta$$

Noting that the length of the flap chord from Fig. 2 and Fig. 4  $b(1-c) = b-\eta$  and using the inverse of the conformal map defined in equation (26),

$$c_l = \sigma_1 \alpha + \sigma_2 \beta \quad (29)$$

where  $\sigma_1, \sigma_2$  are constant value expressions in terms of the geometrical length  $c$  (see Fig. 2).

The aerodynamic moment about an arbitrary point  $x_0$  on the airfoil can be expressed in terms of the strength  $\gamma$  of each elemental vortex as,

$$M = -\rho_\infty v_\infty \int_0^{2b} (\xi - x_0) \gamma(\xi - x_0) d\xi$$

Thin Airfoil Theory provides results [8] for the aerodynamic moment  $M_{ac}$  about the aerodynamic center, which is coincident with the quarter chord point (point 1 in Fig. 2) for a thin airfoil [4]. However, we are interested in the aerodynamic moment  $M_\alpha$  about the elastic center (point 3 in Fig. 2) that appears in equation (12). We proceed by deriving an expression relating  $M_\alpha$  to  $M_{ac}$ . Summing moments about point 3 in Fig. 2,

$$\vec{M}_\alpha = \vec{M}_{ac} + \vec{r}_{13} \times \vec{L} \quad (30)$$

where,  $\vec{r}_{13}$  is the vector from point 1 to 3 and the lift vector  $\vec{L}$  is always orthogonal to the chord line and hence to  $\vec{r}_{13}$ . Also, from Fig. 2,  $|\vec{r}_{13}| = b(\frac{1}{2} + a)$ .

Analogous to the section lift coefficient is the section moment coefficient [4],

$$c_m = \frac{M}{\frac{1}{2}(2b)^2\rho_\infty v_\infty^2} = \frac{M}{2b^2\rho_\infty v_\infty^2} \quad (31)$$

Expressing the moments in equation (30) in terms of moment coefficients (31) and the lift coefficient defined in equation (27),

$$c_{m,\alpha} = c_{m,ac} + \frac{c_l}{2} \left( a + \frac{1}{2} \right) \quad (32)$$

As before,  $c_{m,ac} = c_{m,ac}(\alpha, \beta)$  [4]. Expanding this with a first order Taylor approximation,

$$c_{m,ac}(\alpha, \beta) = c_{m,ac}(0, 0) + \frac{\partial c_{m,ac}}{\partial \alpha} \alpha + \frac{\partial c_{m,ac}}{\partial \beta} \beta \quad (33)$$

The aerodynamic center is a convenient reference because the aerodynamic moment about this point is independent of the angle of attack [4] which implies  $\frac{\partial c_{m,ac}}{\partial \alpha} = 0$  and for a symmetric airfoil,  $c_{m,ac}(0, 0) = 0$  [4]. Thin Airfoil Theory gives constant value expressions [8] ( $\sigma_3, \sigma_4$  in Table 2) for the partial derivatives in equation (33) which are substituted back into equation(32)

Table 2: Thin Airfoil Theory expressions for aerodynamic coefficients

Partial derivative	Symbol	Constant value expression
$\frac{\partial c_l}{\partial \alpha}$	$\sigma_1$	$2\pi$
$\frac{\partial c_l}{\partial \beta}$	$\sigma_2$	$2[\arccos(c) + \sqrt{1-c^2}]$
$\frac{\partial c_{m,ac}}{\partial \alpha}$	$\sigma_3$	0
$\frac{\partial c_{m,ac}}{\partial \beta}$	$\sigma_4$	$-\frac{1}{2}(1+c)\sqrt{1-c^2}$
$\frac{\partial c_{m,\alpha}}{\partial \alpha}$	$\sigma_5$	$\pi\left(\frac{1}{2} + a\right)$
$\frac{\partial c_{m,\alpha}}{\partial \beta}$	$\sigma_6$	$\left(\frac{1}{2} + a\right) \arccos(c) + \left(a - \frac{c}{2}\right) \sqrt{1-c^2}$
$\frac{\partial c_{m,\beta}}{\partial \alpha}$	$\sigma_7$	$\frac{2}{(1-c)^2} \left\{ 2(1+2c) \left( \frac{\pi}{2} - \arccos \sqrt{\frac{1-c}{2}} \right) - (c+2)\sqrt{1-c^2} \right\}$
$\frac{\partial c_{m,\beta}}{\partial \beta}$	$\sigma_8$	$\sigma_7 \left\{ 1 - \frac{1}{\pi} \left( 2 \arccos \sqrt{\frac{1-c}{2}} - \sqrt{1-c^2} \right) \right\} + \left\{ \left[ \frac{4\sigma_4}{\pi(1-c)^2} \right] \left[ \pi - 2 \arccos \sqrt{\frac{1-c}{2}} - \sqrt{1-c^2} \right] \right\}$

along with the expression for  $c_l$  from equation (29) to obtain,

$$c_{m,\alpha} = \sigma_5 \alpha + \sigma_6 \beta \quad (34)$$

where the constant terms  $\sigma_5$ ,  $\sigma_6$  are given in Table 2.

The hinge moment  $M_\beta$  about the flap hinge (point 5 in Fig. 2) arises due to the pressure distribution on the flap. The hinge moment about an arbitrary point  $\tilde{x}_0$  on the flap can be expressed in terms of the strength  $\gamma$  of the elemental vortices arranged along the flap chord as,

$$M_\beta = -\rho_\infty v_\infty \int_{bc}^b (\xi - \tilde{x}_0) \gamma(\xi - \tilde{x}_0) d\eta$$

As before, a section hinge moment coefficient is defined with the airfoil chord  $b$  replaced by the flap chord  $b(1-c)$  (see Fig. 2),

$$c_{m,\beta} = c_{m,\beta}(\alpha, \beta) = \frac{M_\beta}{\frac{1}{2}(b(1-c))^2 \rho_\infty v_\infty^2} \quad (35)$$

From the results of Thin Airfoil Theory [9] we directly obtain expressions for the partial derivatives in the first order Taylor expansion,

$$\begin{aligned} c_{m,\beta}(\alpha, \beta) &= c_{m,\beta}(0, 0) + \frac{\partial c_{m,\beta}}{\partial \alpha} \alpha + \frac{\partial c_{m,\beta}}{\partial \beta} \beta \\ \Rightarrow c_{m,\beta}(\alpha, \beta) &= [\sigma_7 \alpha + \sigma_8 \beta] \end{aligned} \quad (36)$$

Finally, the aerodynamic force and moment expressions from equations (27, 31) can be written in terms of the defined constants from Table 2 as linear functions of  $\alpha$  and  $\beta$ .

$$\begin{aligned} L &= b \rho_\infty v_\infty^2 (\sigma_1 \alpha + \sigma_2 \beta) \\ M_\alpha &= 2b^2 \rho_\infty v_\infty^2 (\sigma_5 \alpha + \sigma_6 \beta) \\ M_\beta &= \frac{1}{2} b^2 (1-c)^2 \rho_\infty v_\infty^2 (\sigma_7 \alpha + \sigma_8 \beta) \end{aligned} \quad (37)$$

## 4 Steady Linear Aeroelastic Model

We combine the aeroelastic equations of motion developed in section 2 with the linear steady aerodynamics developed in section 3 to obtain an aeroelastic model for the system. The model is only as good as the assumptions made and in this case the main limitation is the assumed steadiness of the flow around the airfoil with respect to time. Combining equations (12) and

(37), we write the model equations of motion in matrix form.

$$\begin{aligned}
& \begin{bmatrix} I_\alpha & (I_\beta + b(c-a)S_\beta) & S_\alpha \\ (I_\beta + b(c-a)S_\beta) & I_\beta & S_\beta \\ S_\alpha & S_\beta & m \end{bmatrix} \begin{Bmatrix} \ddot{\alpha} \\ \ddot{\beta} \\ \ddot{h} \end{Bmatrix} + \\
& \begin{bmatrix} k_\alpha - 2b^2\rho_\infty v_\infty^2 \sigma_5 & -2b^2\rho_\infty v_\infty^2 \sigma_6 & 0 \\ -\frac{1}{2}b^2(1-c)^2\rho_\infty v_\infty^2 \sigma_7 & k_\beta - \frac{1}{2}b^2(1-c)^2\rho_\infty v_\infty^2 \sigma_7 & 0 \\ b\rho_\infty v_\infty^2 \sigma_1 & b\rho_\infty v_\infty^2 \sigma_2 & k_h \end{bmatrix} \begin{Bmatrix} \alpha \\ \beta \\ h \end{Bmatrix} = \begin{Bmatrix} 0 \\ 0 \\ 0 \end{Bmatrix} \quad (38)
\end{aligned}$$

Note that the equations are of the general form  $[M]\{\ddot{q}\} + [C]\{\dot{q}\} + [K]\{q\}$ , where  $\{q\}$  is a vector of the system variables, with an overdot representing the time derivative,  $[M]$  is a symmetric inertia matrix,  $[K]$  is a stiffness matrix with contributions from the strain energy of the system, the potential energy of the elastic constraints and contributions from the aerodynamic loads. The matrix  $[C]$  represents the damping present in the system, and is null in this case because of the absence of any dissipative forces in this model. We rewrite the equations in first order form by introducing a change of variables  $\{\alpha, \beta, h, \dot{\alpha}, \dot{\beta}, \dot{h}\} = \{x_1, x_2, x_3, x_4, x_5, x_6\}$ .

$$\begin{aligned}
& \begin{Bmatrix} \dot{x}_1 \\ \dot{x}_2 \\ \dot{x}_3 \\ \dot{x}_4 \\ \dot{x}_5 \\ \dot{x}_6 \end{Bmatrix} = \begin{bmatrix} 0 & 0 & 0 & 1 & 0 & 0 \\ 0 & 0 & 0 & 0 & 1 & 0 \\ 0 & 0 & 0 & 0 & 0 & 1 \\ a_1 v_\infty^2 + b_1 & a_2 v_\infty^2 + b_2 & b_3 & 0 & 0 & 0 \\ a_3 v_\infty^2 + b_4 & a_4 v_\infty^2 + b_5 & b_6 & 0 & 0 & 0 \\ a_5 v_\infty^2 + b_7 & a_6 v_\infty^2 + b_8 & b_9 & 0 & 0 & 0 \end{bmatrix} \begin{Bmatrix} x_1 \\ x_2 \\ x_3 \\ x_4 \\ x_5 \\ x_6 \end{Bmatrix} \quad (39)
\end{aligned}$$

This linear, 2nd order ODE has solutions of the form  $\vec{x}(t) = \vec{v}e^{\lambda t}$ , where  $\lambda$  is an eigenvalue of the system given above with an associated eigenvector  $\vec{v}$ . The velocity  $v_\infty$  is shown explicitly in the matrix because of its importance

in this analysis. Prediction and characterization of the flutter boundary is our ultimate goal and the system behavior is studied for various values of  $v_\infty$ . The constants  $a_i$ ,  $i = 1, 2 \dots, 6$  and  $b_j$ ,  $j = 1, 2 \dots, 9$  are expressions of the system constants from Table 1. Numerical values for a real airfoil geometry with corresponding physical structural data, obtained from experimental results published in reference [10], are tabulated in Table 3. These numbers were used to numerically integrate the ODEs in equation (39) using a 4th order Runge-Kutta scheme with a 5th order correction. The airflow density was taken to be that at mean sea level. The numerics correspond to a physical situation where an airfoil is flown at sea level between speeds of 0 to 100  $m/s$ . The limitations on the speed are a direct consequence of the incompressible, inviscid assumptions made in the aerodynamic model, (see section 3) which only hold for a Mach number of  $M < 0.3$ , corresponding to an airflow velocity of  $v_\infty \approx 100m/s$ . The airfoil was chosen to run at sea level because of this speed limitation in order to reflect a real physical regime in which aircraft operate - the takeoff roll. This usually occurs at speeds within the limits of our model at sea level. Speeds at the high end of this range are also normal for the initial ascent of small, low speed private commuter aircraft like the Cessna series of single engine turboprops.

The six eigenvalues of the system take the form  $\Gamma_k \pm i\Omega_k$ ,  $k = 1, 2, 3$ , where the stability of the system is strongly dependent on the real part of the eigenvalues,  $\Gamma_k$ . The stability of the system is ensured for  $\Gamma_k \leq 0$ . The system exhibits oscillatory behavior for non-zero values of the imaginary part  $\Omega_k$ . The response for the set of parameters given in Table 3 is dynamically unstable over a significant range of velocities within the limit of the model, with highly divergent and unbounded oscillations increasing with time. The behavior of the imaginary part of the eigenvalues with changes in airflow

Table 3: Physical Data

<b>Structural Constants</b>	
$b$	0.127 <i>m</i>
$m$	1.567 <i>kg</i>
$I_\alpha$	0.01347 <i>kgm</i> <sup>2</sup>
$I_\beta$	0.0003264 <i>kgm</i> <sup>2</sup>
$S_\alpha$	0.08587 <i>kgm</i>
$S_\beta$	0.00395 <i>kgm</i>
$k_\alpha$	37.3 <i>kgm/s</i> <sup>2</sup>
$k_\beta$	39 <i>kgm/s</i> <sup>2</sup>
$k_h$	2818.8 <i>kgm/s</i> <sup>2</sup>
$\rho_\infty$	1.225 <i>kg/m</i> <sup>3</sup>
<b>Geometrical Constants (Non-dimensional)</b>	
$a$	-0.5
$c$	0.5

speed is shown in Figure 5. A plot of the real part  $\Gamma_k$  versus  $v_\infty$  shown in Figure 6, shows that the first bifurcation occurs at a value of  $v_\infty \approx 25 \text{ m/s}$ , where  $\Gamma_k$  first take a positive value. This bifurcation corresponds to a change in the stability of the system from stable to divergent oscillations and is the predicted flutter boundary. The onset of flutter at such an early stage in the flight regime is highly undesirable since most modern aircraft takeoff at speeds  $\sim 60 \text{ m/s}$ . We seek to tailor the design of the airfoil such that flutter is delayed as long as possible. Within the limits of the present model, a flutter speed above  $100 \text{ m/s}$  would be a good design objective because beyond this speed the model will no longer produce meaningful results.

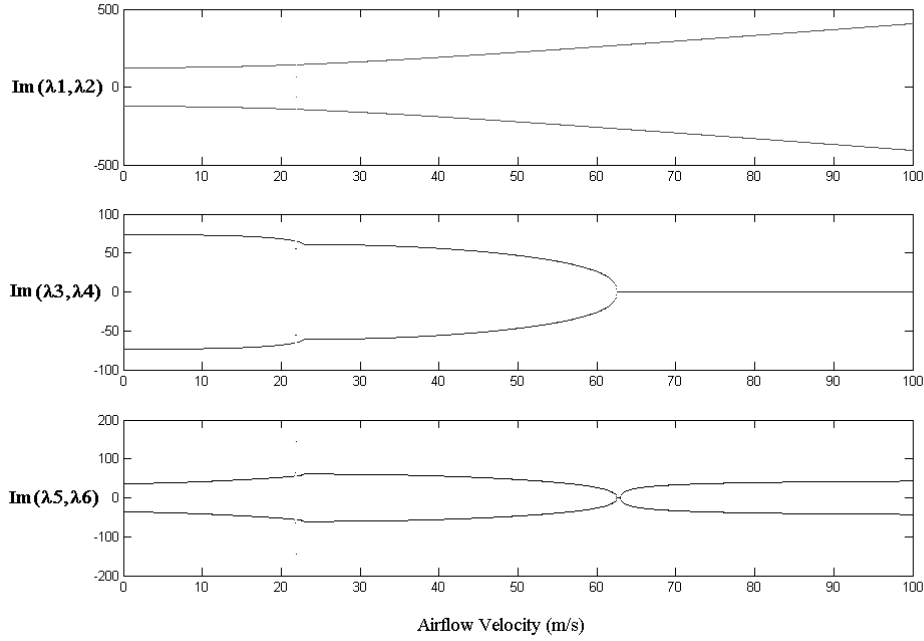


Figure 5: Imaginary part of eigenvalues plotted versus flow speed (in m/s). See [10] for airfoil data. See Table 3 for values of system constants. The system dynamics for this configuration are highly unstable divergent oscillations.

The criterion used to determine the first occurrence of flutter is the appearance of the first bifurcation point in the  $\Gamma_k$  plot. Stability corresponds to a zero or negative  $\Gamma_k$  for all values of  $v_\infty$  within the boundaries of the model. With this design goal in mind, the behavior of the system was studied for changes in various model parameters. The first approach adopted was in varying the geometrical configuration of the airfoil. The location of the elastic center (point 3 in Fig. 2), corresponding to the value of  $a$  in Table 3 had no significant effect on the location of the first bifurcation point. The location of the airfoil CG (point 4 in Fig. 2) with respect to the elastic center

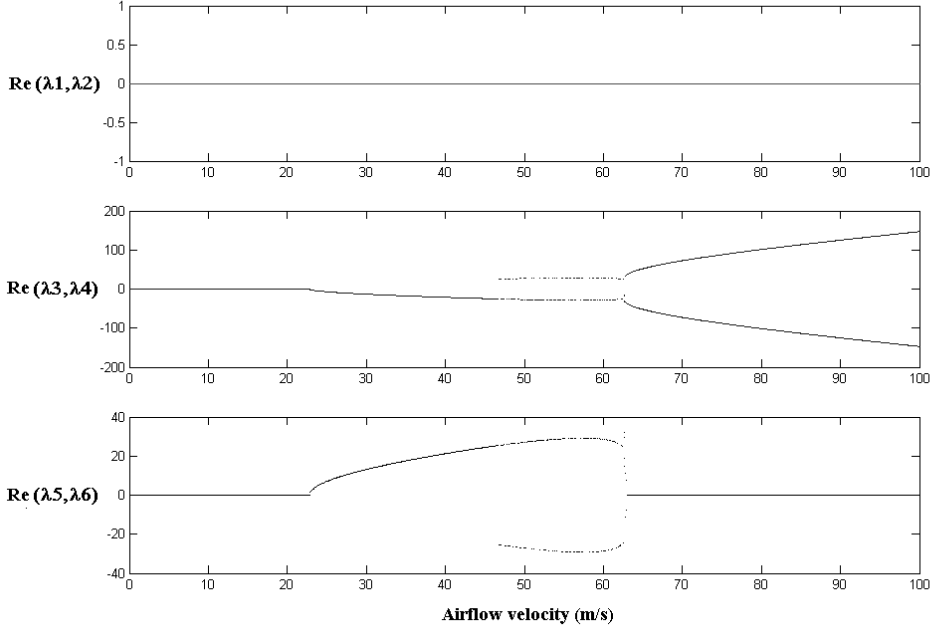


Figure 6: Real part of eigenvalues plotted versus flow speed (in m/s). Note the first bifurcation for  $v_\infty \approx 25$  m/s. This is the predicted flutter velocity. See [10] for airfoil data. See Table 3 for values of system constants. The system dynamics for this configuration are highly unstable divergent oscillations.

was then changed. This corresponds to an increase or decrease in the static moment  $S_\alpha$  (see Table 1 and equation (7) for definitions). Increasing  $S_\alpha$  which implies moving the center of gravity towards the TE of the airfoil only worsened the situation with flutter occurring at even lower speeds. A decrease in  $S_\alpha$ , obtained by moving the CG towards the LE of the airfoil did delay the onset of the first bifurcation. However, the flutter boundary was still within 100 m/s for the maximum decrease in  $S_\alpha$  possible physically. For example, the flutter boundary was pushed forward to around 70 m/s for

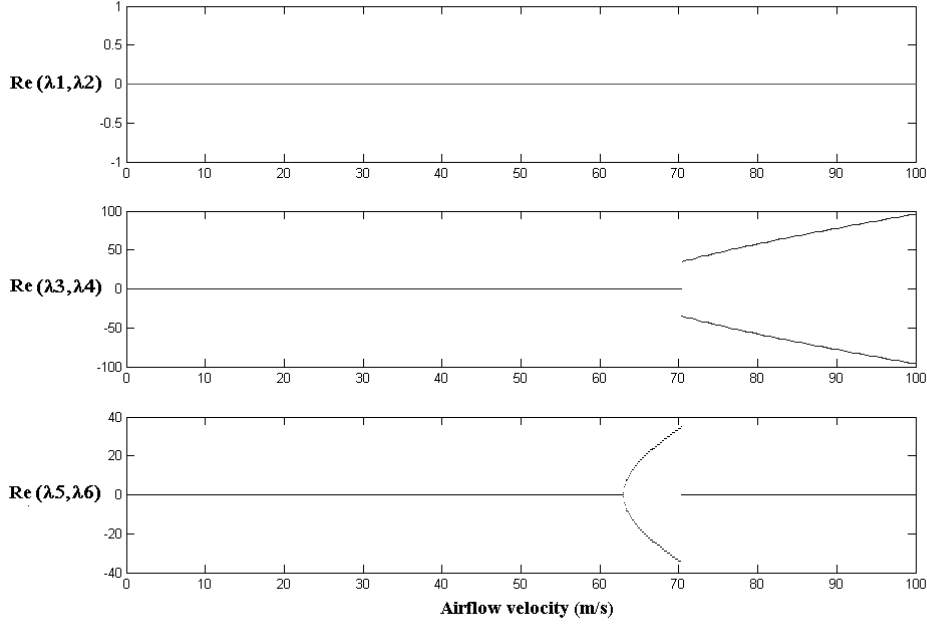


Figure 7: Real part of eigenvalues plotted versus flow speed (in m/s).  $S_\alpha = 0.008587 \text{ kgm}$ . Note the delayed first bifurcation for  $v_\infty \approx 65 \text{ m/s}$ , when compared to Fig. 6. However, flutter is still predicted before the model limit of  $v_\infty = 100 \text{ m/s}$

10% of the original  $S_\alpha$  (see Fig. 7).

The second configuration change was altering the structural characteristics of the airfoil. The stiffness of the airfoil constraints in pitch, plunge and flap were changed. This approach was successful and the flutter boundary was pushed outside the physical envelope of this model. Combining a change in the geometry of the airfoil with a change in its structural stiffness produced the best results for the smallest alteration in the airfoil configuration. For example, a 250% increase in  $k_\alpha$  and  $k_\beta$  changing the stiffness of

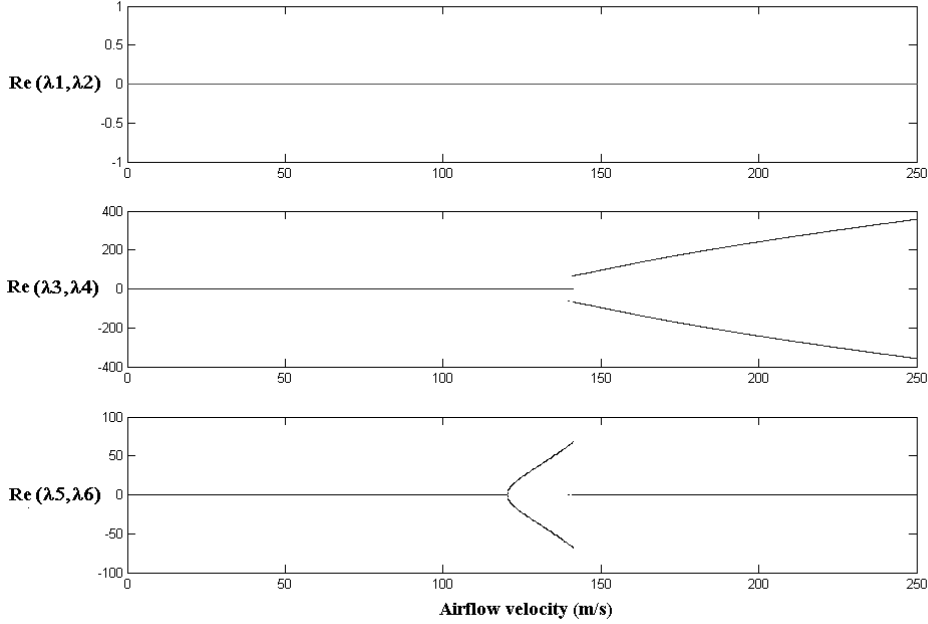


Figure 8: Real part of eigenvalues plotted versus flow speed (in  $m/s$ ).  $S_\alpha = 0.008587 \text{ kgm}$ ,  $k_\alpha = 93.25 \text{ kgm/s}^2$ ,  $k_\beta = 97.5 \text{ kgm/s}^2$ . The airfoil stiffness has been increased by 250% and the CG is shifted forward towards the LE by 90%. Note the first bifurcation for  $v_\infty \approx 125 \text{ m/s}$  falls outside the boundaries of the model ( $v_\infty < 100 \text{ m/s}$ ).

the airfoil in pitch and flap, combined with a 50% decrease in  $S_\alpha$  produced the first bifurcation at a speed of around  $120 \text{ m/s}$ , thus ensuring no flutter within our desired speed envelope. The bifurcation diagram is shown in Figure 8 with the imaginary parts of the eigenvalues plotted in Figure 9. The stable oscillatory behavior of the system for the new parameters is shown in Figure 10.

The above analysis is deficient because of the shortcomings of the aero-

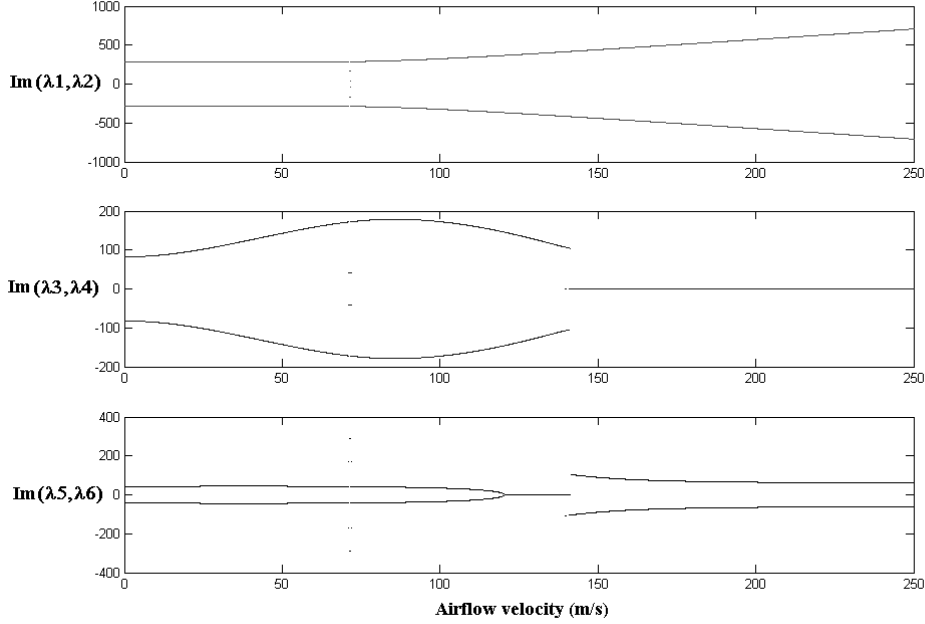


Figure 9: Imaginary part of eigenvalues plotted versus flow speed (in  $m/s$ ).  $S_\alpha = 0.008587 \text{ kgm}$ ,  $k_\alpha = 93.25 \text{ kgm/s}^2$ ,  $k_\beta = 97.5 \text{ kgm/s}^2$ . The airfoil stiffness has been increased by 250% and the CG is shifted forward towards the LE by 90%. There is no predicted flutter within the boundaries of the model ( $v_\infty < 100 \text{ m/s}$ ).

dynamic model chosen. While the linear nature of the aerodynamics is one major limiting assumption, the major obstacle to obtaining a realistic picture of the dynamics is due to the absence of dissipative forces. The flow around the airfoil changes with time and thus physically accurate predictions flutter speed can only be made using unsteady aerodynamics [1]. However, at least some qualitative inferences can be made from this limited model. The flutter speed dependence on the bifurcation point of the real part of

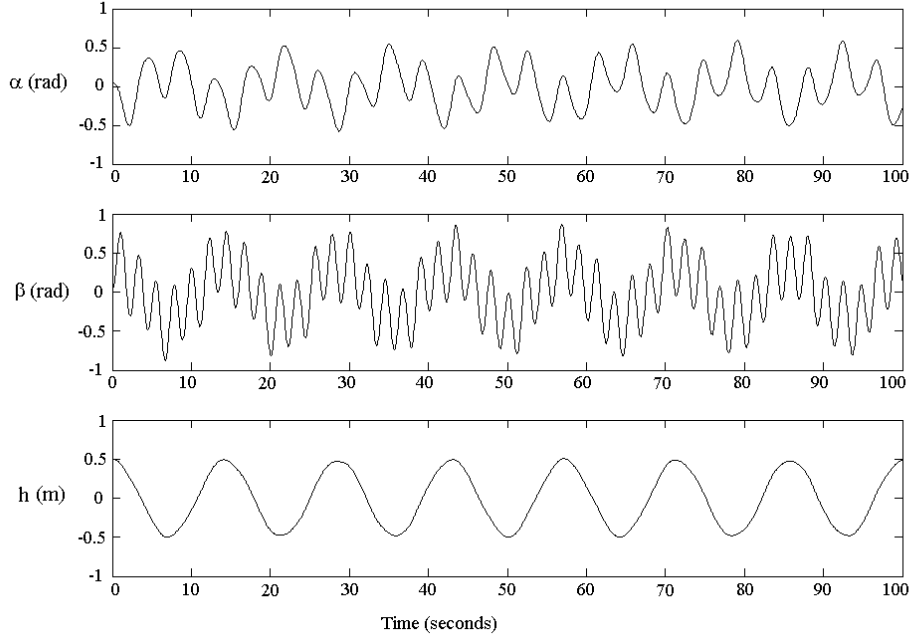


Figure 10: System dynamics for a simulation time of 100 seconds.  $S_\alpha = 0.008587 \text{ kgm}$ ,  $k_\alpha = 93.25 \text{ kgm/s}^2$ ,  $k_\beta = 97.5 \text{ kgm/s}^2$ . Note that the oscillations do not diverge. The maximum deflection of the airfoil is about 0.5 m, which is twice the airfoil length. The pitch and flap oscillations are also within 1 radian.

the system eigenvalues has been established. It is also evidently possible to delay the onset of instability by changing the structure of the airfoil. For example, moving the CG location of the airfoil forward with respect to its elastic axis, towards the LE, while stiffening the airfoil structurally leads to an increase in the flutter speed for the linear aerodynamic model chosen.

## 5 Concluding Remarks

In this paper, a linear steady state aeroelastic model in 3 DOF was derived *a priori* for a 2 dimensional airfoil model. The equations of motion were derived from the Lagrangian formulation for conservative systems. A flutter boundary was predicted at sea level conditions and the effects of airfoil geometry and structural characteristics on the predicted value were studied. The results indicate that a linear steady state model cannot accurately predict the flutter boundary. The weakness in the model lies entirely in the assumed steadiness of the airflow around an airfoil. There are several perturbative effects introduced into the flow due to the movement of the airfoil that are entirely neglected. Furthermore, the steady state assumption limits the velocity range for which this model is valid, due to the necessary preconditions of inviscidity and incompressibility that have been introduced while deriving the aerodynamical model. However, the model does provide a certain amount of insight into the nature of the flutter boundary. It is shown that the flutter boundary can be inferred from the behavior of the real part of the eigenvalues arising from the equations of motion. It has also been noticed that changing certain airfoil structural and geometrical parameters leads to a shift in the position of the flutter boundary. This is significant because it allows for the design of an airfoil which will never encounter flutter for a certain flight regime.

The development of unsteady aerodynamics to complement the structural equations derived earlier in this paper is the logical next step. The introduction of dissipative forces into the flow around an airfoil will lead to a more realistic prediction of flutter characteristics. A readily available and widely used [1] unsteady aerodynamic theory is Peters' finite state,

induced-flow theory. Subsequent work should include results from this theory in the aerodynamics of the model derived in this paper. In Peters' theory, the aerodynamic forcing functions can be expressed as functions of time derivatives of the system variables, such that  $L = L(\alpha, \beta, h, \dot{\alpha}, \dot{\beta}, \dot{h})$ ,  $M_\alpha = M_\alpha(\alpha, \beta, h, \dot{\alpha}, \dot{\beta}, \dot{h})$ ,  $M_\beta = M_\beta(\alpha, \beta, h, \dot{\alpha}, \dot{\beta}, \dot{h})$ . The second step will be incorporating structural nonlinearities into the unsteady model. This will be effected by replacing the structural stiffness constants  $k_\alpha, k_\beta, k_h$  with polynomial stiffness coefficients  $k_\alpha(\alpha), k_\beta(\beta), k_h(h)$ .

## Acknowledgements

I would like to thank my undergraduate research advisor Dr. Mason Porter of the School of Mathematics and Dr. Slaven Peles of the Center for Non-linear Science in the School of Physics for their guidance and support. I am grateful to Dr. Dewey Hodges and my undergraduate advisor Dr. Marilyn Smith of the School of Aerospace Engineering for their invaluable advice.

## References

- [1] Dewey H. Hodges and G. Alvin Pierce. *Introduction to Structural Dynamics and Aeroelasticity*. Cambridge University Press, first edition, 2002.
- [2] Theodore Theodorsen. General theory of aerodynamic instability and the mechanism of flutter. NACA Technical Report 496, 1935.
- [3] B.H.K. Lee, S.J. Price, and Y.S. Wong. Nonlinear aeroelastic analysis of airfoils: bifurcation and chaos. *Progress in Aerospace Sciences*, (35):205–334, 1999.

- [4] John D. Anderson Jr. *Fundamentals of Aerodynamics*. McGraw-Hill, third edition, 2001.
- [5] Ira H. Abbott and Albert E. von Doenhoff. *Theory of Wing Sections*. Dover Publications, first dover edition, 1959.
- [6] Herbert Goldstein, Charles P. Poole Jr, and John L. Safko. *Classical Mechanics*. Addison Wesley, third edition, 2003.
- [7] Frank M. White. *Fluid Mechanics*. Mc Graw Hill, fifth edition, 2002.
- [8] Arnold M. Kuethe and Chuen-Yen Chow. *Foundations of Aerodynamics - Bases of Aerodynamic Design*. John Wiley and Sons, fifth edition, 1998.
- [9] Hermann Glauert. Theoretical relationships for an aerofoil with hinged flap. ARC Reports and Memoranda 1095, Aeronautical Research Committee, 1927.
- [10] E.H. Dowell, J.P. Thomas, and K.C. Hall. Transonic limit cycle oscillation analysis using reduced order aerodynamic models. *Journal of Fluids and Structures*, (19):17–27, 2004.